



# A Review of Source Models of the 2015 Illapel, Chile Earthquake and Insights from Tsunami Data

KENJI SATAKE<sup>1</sup>  and MOHAMMAD HEIDARZADEH<sup>1,2</sup>

**Abstract**—The 16 September 2015 Illapel, Chile, earthquake and associated tsunami have been studied by many researchers from various aspects. This paper reviews studies on the source model of the earthquake and examines tsunami data. The Illapel earthquake occurred in the source region of previous earthquakes in 1943 and 1880. The earthquake source was studied using various geophysical data, such as near-field seismograms, teleseismic waveform and backprojection, GPS and InSAR data, and tsunami waveforms. Most seismological analyses show a duration of  $\sim 100$  s with a peak at  $\sim 50$  s. The spatial distribution has some variety, but they all have the largest slip varying from 5 to 16 m located at  $31^\circ\text{S}$ ,  $72^\circ\text{W}$ , which is  $\sim 70$  km NW of the epicenter. The shallow slip seems to be extended to the trench axis. A deeper slip patch was proposed from high-frequency seismic data. A tsunami earthquake model with a total duration of 250 s and a third asperity south of the epicenter is also proposed, but we show that the tsunami data do not support this model.

**Key words:** 2015 Illapel earthquake, tsunami, earthquake source model, Pacific Ocean, Chilean earthquakes.

## 1. Introduction

Many great earthquakes repeatedly occur offshore Chile, where Nazca plate subducts beneath the South American plate (Fig. 1). This seismic zone hosted the largest earthquake ever recorded, the 22 May 1960 Valdivia earthquake ( $M_w$  9.5, Kanamori 1977) that occurred in southern Chile. In northern and central Chile, three great tsunamigenic earthquakes occurred in the last decade (Fig. 1): the 27 February 2010 Maule earthquake ( $M_w$  8.8, Global CMT) with more than 500 deaths as a result of both the earthquake and associated tsunami, the 1 April

2014 Iquique earthquake ( $M_w$  8.1, Global CMT), and the 16 September 2015 Illapel earthquake ( $M_w$  8.3, Global CMT). The 2015 Illapel earthquake occurred at 22:54:32 (UT) on 16 September, at  $31.573^\circ\text{S}$ ,  $72.674^\circ\text{W}$  at 22.4 km depth, according to the United States Geological Survey. The global centroid moment tensor (CMT) catalogue provided the scalar seismic moment of  $3.2 \times 10^{21}$  Nm. Its focal mechanism solution is strike:  $7^\circ$ , dip:  $19^\circ$ , and rake:  $109^\circ$ , indicating thrust-type faulting having its strike parallel to the trench.

Source regions and recurrence of great earthquakes offshore Chile have been studied based on historical, seismological, and tsunami data (Kelleher 1972; Comte and Pardo 1991; Beck et al. 1998). The 2010 Maule earthquake is considered to be a re-rupture of the 1835 earthquake, which was documented by Darwin during his voyage on Beagle (Madariaga et al. 2010). The rupture length of the 2014 Iquique earthquake was about 200 km, and it was only a part of that of the previous great earthquake of 1877 (Schurr et al. 2014; Gusman et al. 2015; Lay et al. 2014).

In the source region of the 2015 Illapel earthquake, similar earthquakes occurred in 1943 and 1880 and a larger earthquake in 1730 (Fig. 1, Ruiz et al. 2016). The 2015 Illapel earthquake is considered to be a re-rupture of the 1943 earthquake ( $M_w$  7.9, Beck et al. 1998). Tsunami from the 1943 earthquake was recorded in Japan with height of 10 cm in Hanasaki and 25 cm in Kushimoto (Hatori 1968; Watanabe 1998). To the north of the 2015 source region, the tsunamigenic Atacama earthquake ( $M_s$  8.3) occurred in 1922 (Beck et al. 1998) as well as in 1819. The region south of the 2015 source was ruptured by the 1971

<sup>1</sup> Earthquake Research Institute, The University of Tokyo, Tokyo, Japan. E-mail: satake@eri.u-tokyo.ac.jp

<sup>2</sup> Port and Airport Research Institute, Yokosuka, Japan.

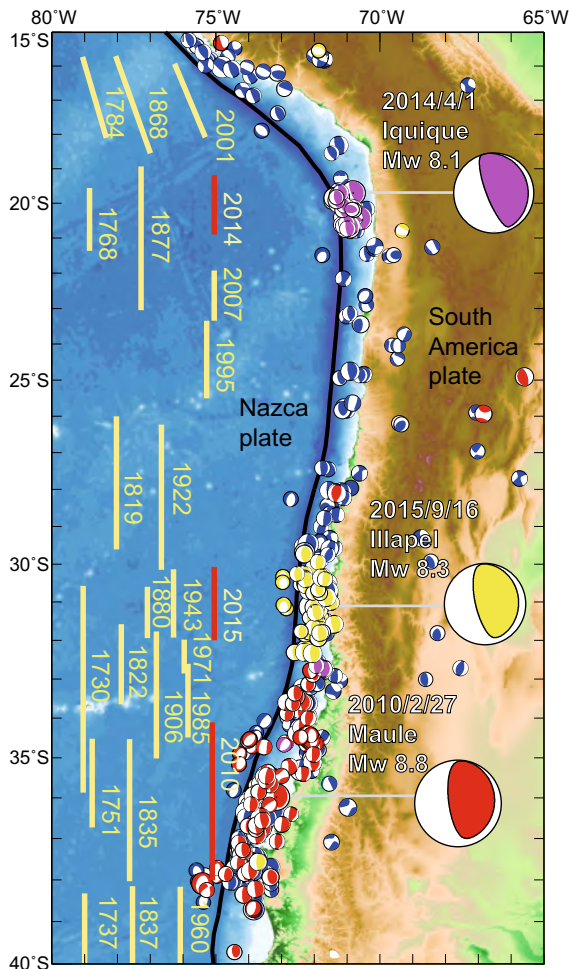


Figure 1

Focal mechanism solutions of Global CMT project for shallow (depth <100 km) earthquakes between 2010 and 2015. Those in red, purple, and yellow colors are earthquakes that occurred within 1 month of the three great earthquakes (2010 Maule, 2014 Iquique, and 2015 Illapel). Source zones of historical earthquakes are shown in bars (Kelleher 1972; Comte and Pardo 1991; Beck et al. 1998; Schurr et al. 2014)

( $M$  7.8, USGS) and 1985 ( $M$  8.0, USGS) Valparaíso earthquakes and by the 1906 great earthquake ( $M_s$  8.4) (Ye et al. 2016).

Interseismic coupling along the Chilean plate boundary has been inferred from dense GPS networks, operated by Chilean collaborations with American, French, and German groups. High- and low-coupling zones have been identified. The source regions of recent large earthquakes match with highly coupled segments (e.g., Moreno et al. 2010; Schurr et al. 2014; Métois et al. 2016).

## 2. Tsunami Data

The great earthquakes offshore Chile have generated tsunamis, which caused damage not only on the Chilean coast but also across the Pacific Ocean. The 1960 Chilean earthquake and tsunami killed 2000 people on the Chilean coast (Atwater et al. 1999). The tsunami caused 61 and 142 fatalities in Hawaii and Japan, respectively (Atwater et al. 1999; Watanabe 1998). The tsunami heights from the 2010 Maule earthquake were mostly up to 15 m on the Chilean coast, and the total fatalities were 156. The tsunami height was <2 m on the Japanese coast, but caused some property damage (Fujii and Satake 2013).

The 2015 Illapel earthquake generated local and trans-Pacific tsunami (Aránguiz et al. 2016; Contreras-López et al. 2016; Tang et al. 2016; Zaytsev et al. 2016). Along the Chilean coast, the Pacific Tsunami Warning Center (PTWC) and National Hydrographic and Oceanic Service (SHOA) issued tsunami threat messages 7 and 8 min following the earthquake, respectively (Aránguiz et al. 2016). Such prompt messages and evacuation helped to minimize tsunami fatalities (eight deaths according to Aránguiz et al. 2016).

The post-tsunami surveys measured tsunami heights on the Chilean coast (Aránguiz et al. 2016; Contreras-López et al. 2016). The maximum runup height was reported as 10.8 m at Totoral (30.37°S) by Aránguiz et al. (2016), whereas it was 13.6 m at La Cebada (30.97°S) by Contreras-López et al. (2016). Except for such anomalous locations, the tsunami heights were up to 9 m on the coast between 29°S and 32°S, and smaller further south and north (Fig. 2).

The tsunami was also recorded on coastal tide gauges (Aránguiz et al. 2016; Heidarzadeh et al. 2016). The earliest tsunami arrival of ~15 min with zero-to-peak amplitude of <2 m was recorded at Pichidangui tide gauge station, just south of the epicenter. To the north, at Coquimbo tide gauge station, the first arrival was at 23 min with ~1 m amplitude, but the largest tsunami amplitude of 4.7 m was recorded ~1.5 h after the earthquake. Omira et al. (2016) made a comparison of the near-field tsunami records from the three earthquakes.

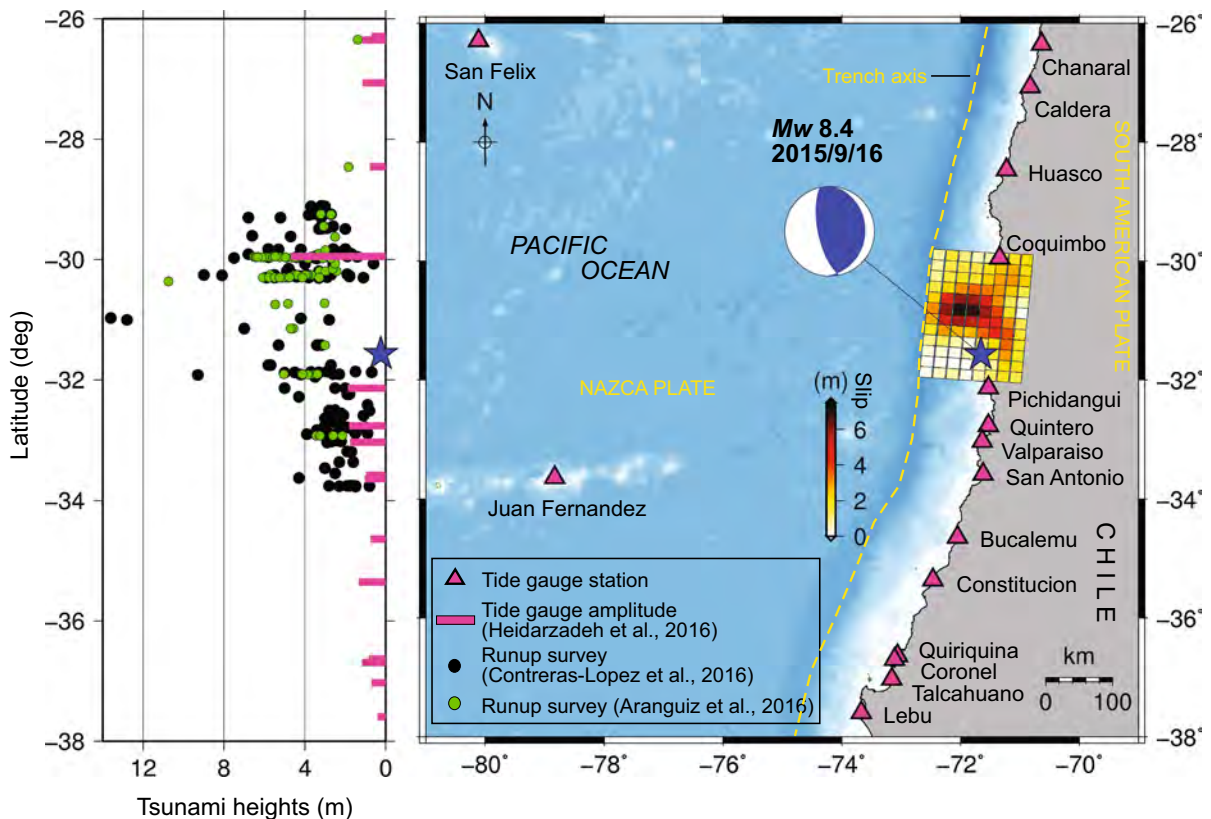


Figure 2

Maximum tide gauge amplitudes of the 2015 Illapel tsunami (pink columns after Heidarzadeh et al. 2016) along with the tsunami heights reported by Aránguiz et al. (2016) (green circles) and Contreras-López et al. (2016) (black circles). The slip model is from Heidarzadeh et al. (2016)

While the tide gauge tsunami amplitudes vary in the range 1–2 m with a maximum value of 4.7 m, runup heights are in the range 3–6 m with a maximum value of ~11–14 m (Fig. 2). Tsunami runup heights are roughly up to three times of the tide gauge amplitudes along the Chilean coast.

According to NOAA Global Historical Tsunami Database (doi:10.7289/V5PN93H7, [https://www.ngdc.noaa.gov/hazard/tsu\\_db.shtml](https://www.ngdc.noaa.gov/hazard/tsu_db.shtml), accessed on 24 October 2016), the tsunami heights across the Pacific Ocean were as follows: 1.37 m in Marquesas Islands, 0.83 m in Hawaii (Hilo), 0.52 m in New Zealand (Chatham), and 0.10 m in Australia (Port Kembla). In Japan, Japan Meteorological Agency issued tsunami advisory at 18:00 on September 17 (UT), approximately 19 h after the earthquake and 3 h before the first tsunami arrival to Japan, with expected tsunami

heights of <1 m. The largest observed tsunami amplitude was 0.78 m on Kuji GPS buoy.

The tsunami was also recorded in deep ocean on Deep-ocean Assessment and Reporting of Tsunamis (DART) buoys. Figure 3 compares the tsunami waveforms recorded at four DART stations from the recent three earthquakes. At station 32412, offshore Peru, the 2015 tsunami arrived at ~2.7 h following the earthquake. The 2015 tsunami amplitude was ~10 cm, about the same as tsunami from the 2014 Iquique earthquake and about a half of that from the 2010 Maule earthquake. At stations 43412 off Mexico and 46409 in the Aleutians, the 2015 tsunami arrived at 9 and 17 h after the earthquake, respectively, and the amplitude was a few cm, much smaller than the 2010 tsunami and slightly smaller than the 2014

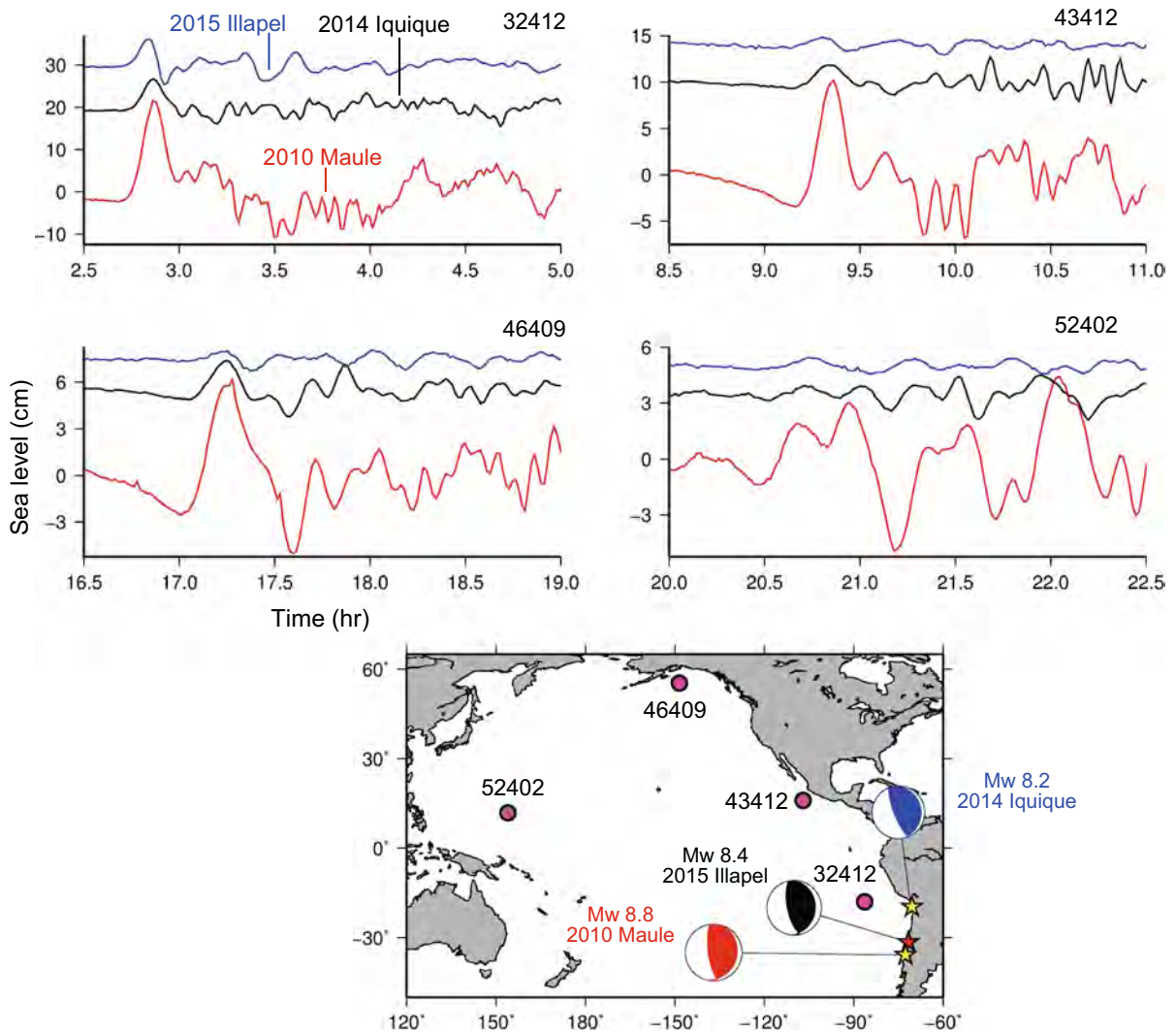


Figure 3

Tsunami waveforms from the recent three great earthquakes recorded at four DART stations. The time on the horizontal axis is from the earthquake origin time only for the 2015 Illapel tsunami (the *blue waveforms*). The waveforms for the other two tsunamis (*red and black waveforms*) are shifted in time to align the first peaks

tsunami. At station 52402 near Saipan in the western Pacific Ocean, the 2015 tsunami arrived at around 20.5 h. The tsunami amplitudes were a few cm from the 2010 earthquake and almost noise level for the 2014 and 2015 earthquakes. These tsunami waveforms, combined with seismological and geodetic data, are used to study the source process of these earthquakes (Fujii and Satake 2013; Yoshimoto et al. 2016; Gusman et al. 2015; Heidarzadeh et al. 2015).

### 3. Slip Distribution

The slip distribution of the 2015 Illapel earthquake was studied using various observation data, such as near-field seismic data, teleseismic waveforms, geodetic data, and tsunami waveforms.

Heidarzadeh et al. (2016) used teleseismic and tsunami waveforms to estimate the slip distribution. They first conducted teleseismic waveform inversion by assuming various maximum rupture velocities.

The source time (moment rate) functions and the waveform fits of observed and synthetic waveforms are insensitive to the choice of rupture velocity and they are similar for different rupture velocities. The source time function indicates rupture duration of  $\sim 120$  s with the peak at  $\sim 50$  s. However, the spatial distribution of coseismic slip, the resultant seafloor deformation, and computed tsunami waveforms is different for different rupture velocities. By comparing with the observed tsunami waveforms, they concluded that the slip model with assumed rupture velocity of 1.75 km/s best explains the observed tsunamis waveforms. This model has a large-slip area of 80 km along strike and 100 km along dip, and the peak slip is located at around  $31^\circ\text{S}$ ,  $72^\circ\text{W}$ , approximately 70 km from the trench axis and  $\sim 70$  km northwest of the epicenter (Fig. 4a). The average slip of the large-slip area is 5.0 m and the total seismic moment is  $4.42 \times 10^{21}$  Nm ( $M_w$  8.4).

Li et al. (2016) also used teleseismic and tsunami waveforms to estimate slip distribution. Their slip model is basically similar to that of Heidarzadeh et al. (2016), but the large-slip area extended in the north-south direction with a total length of 170 km, and the peak slip is almost 10 m and located closer to the trench (Fig. 4b). The total seismic moment is  $2.6 \times 10^{21}$  Nm ( $M_w$  8.2).

Ruiz et al. (2016) used the high-rate GPS data at 15 stations to estimate the coseismic slip distribution. The result is similar to the slip models obtained from tsunami and seismic waveform data, with the peak slip of 7 m located at around  $31^\circ\text{S}$ ,  $72^\circ\text{W}$  (Fig. 4c), and the total moment of  $4.2 \times 10^{21}$  Nm ( $M_w$  8.3). Zhang et al. (2016) used SAR Interferometry (InSAR) data to estimate a similar peak, with reverse dip-slip and right-lateral strike-slip components of 8.3 and 1.5 m, respectively. The seismic moment is estimated at  $3.3 \times 10^{21}$  Nm ( $M_w$  8.3).

Tilman et al. (2016) made a joint inversion of geodetic and teleseismic backprojection data. Their slip model also has the peak at  $31^\circ\text{S}$  but with a value of 4.8 m (Fig. 3d). The peak slip is less localized than in the other models.

Melgar et al. (2016) used near-field seismic, geodetic, and tsunami data, as well as teleseismic backprojection data, and showed two areas of large slip (asperities). They are both around  $31^\circ\text{S}$ ; the

shallow one is west of  $72^\circ\text{W}$  and the deep one is east of  $72^\circ\text{W}$ . The deep asperity extends to 45 km depth with 10 m peak slip at 30 km depth. The shallow asperity extends to the trench with  $\sim 10$  m peak slip at 15 km depth. About 5 m slip occurred for 200 km along the trench (Fig. 4e). Li and Ghosh (2016) also applied teleseismic backprojection but mapped three patches located around, to the northeast of, and to the northwest of the epicenter. Okuwaki et al. (2016) made a hybrid inversion of teleseismic waveform and backprojection data, and found secondary high-frequency sources in the deeper part of the rupture area.

Lee et al. (2016) inverted teleseismic data with Green's functions computed with a 3D spectral-element method. They showed that the rupture occurred in two stages. During the first stage with duration of  $\sim 100$  s, asperities I and II ruptured (see Fig. 4f for locations). These two asperities are similar to those of Melgar et al. (2016), but the slips are larger: the peak slips of asperities I and II are 10, and 16 m, respectively (Fig. 4f). The total seismic moment of the first stage is  $3.8 \times 10^{21}$  Nm ( $M_w$  8.3). What is unique about their model is the second stage, which starts at 100 s after the start of the first stage and lasts until 250 s. They propose that the second stage is a slow rupture at offshore asperity III, south of the epicenter. The second stage has a peak slip of 6 m and a seismic moment of  $1.7 \times 10^{21}$  Nm (equivalent to  $M_w$  8.1). They consider the first stage a typical interplate earthquake while the second stage a tsunami earthquake. The total seismic moment is  $5.5 \times 10^{21}$  Nm ( $M_w$  8.4) which is close to that of Heidarzadeh et al. (2016) and other studies.

To summarize various slip models, most seismological studies report the total duration of  $\sim 100$  s with a peak at  $\sim 50$  s for the 2015 Illapel earthquake. The spatial distribution has some variety, but they all have the largest slip located at  $31^\circ\text{S}$ ,  $72^\circ\text{W}$ , and  $\sim 70$  km NW of the epicenter, but the slip amount varies from 5 to 16 m, nearly a factor of three. The difference in the largest slip may be due to different subfault size; it is not the slip on the fault but the seismic moment that controls the amplitudes of seismic waves, and the seafloor displacements (slip and fault area) that controls tsunami amplitudes. The shallow slip seems to be extended to the trench axis. A deeper slip patch was proposed from high-

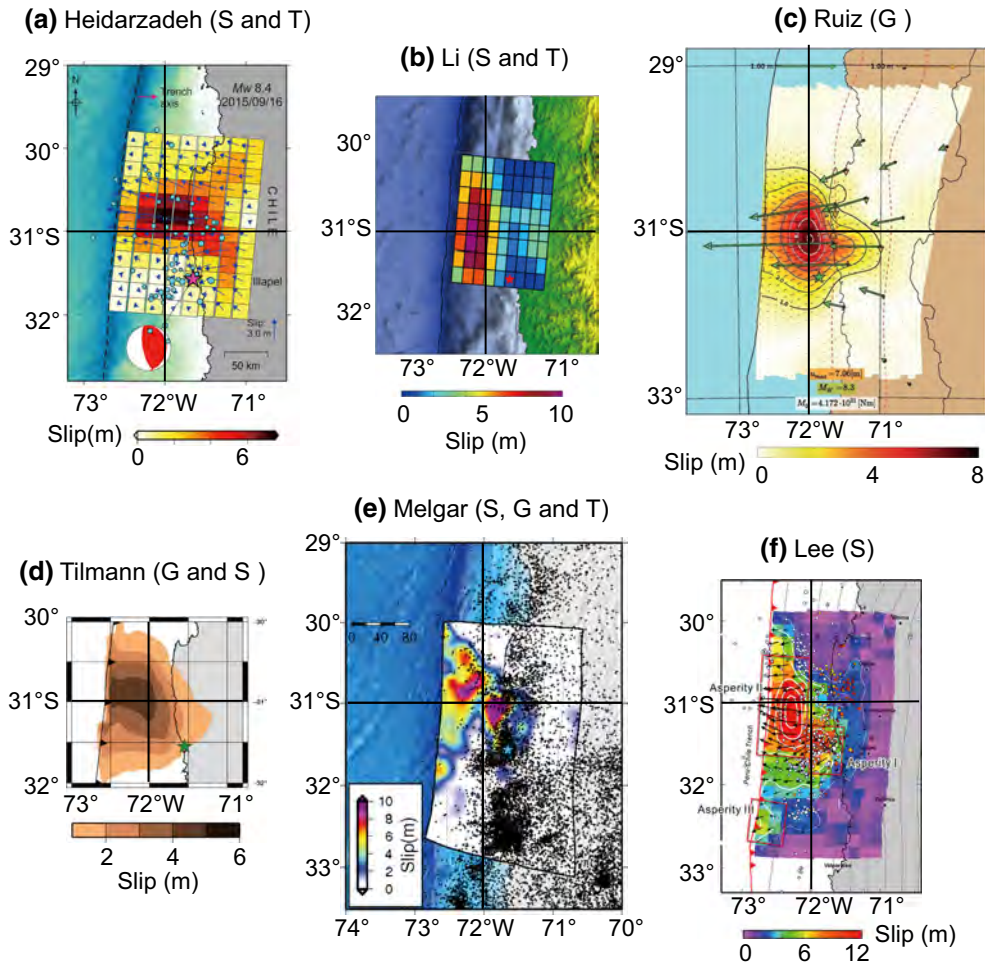


Figure 4

Six slip distribution models estimated by various data sets. *S*, *T*, and *G* stand for seismic, tsunami, and geodetic data, respectively. References are **a** Heidarzadeh et al. (2016), **b** Li et al. (2016), **c** Ruiz et al. (2016), **d** Tilmann et al. (2016), **e** Melgar et al. (2016), and **f** Lee et al. (2016)

frequency seismic waves. A model of regular earthquake followed by a tsunami earthquake with a total duration of 250 s and a third asperity south of the epicenter is proposed by Lee et al. (2016).

Tsunami modeling for different seismic sources and comparison with observations were carried out by Calisto et al. (2016) and Fuentes et al. (2016).

#### 4. Insights from Tsunami Data

The locations of maximum tsunami runups reported by Aránguiz et al. (2016) and Contreras-López et al. (2016) are at the distances of  $\sim 130$  and

$\sim 70$  km to the north of epicenter, respectively (Fig. 2). The largest tsunami heights, both runup and tide gauge heights, are concentrated at around latitude of  $31^\circ\text{S}$  which corresponds to the zone of maximum slip (Fig. 2). In addition, tsunami heights to the north of the epicenter are larger than those to the south (Fig. 2), possibly confirming the northward propagation of the earthquake rupture from the epicenter as reported by most seismological studies.

The main tsunami source can be estimated from the travel time of tsunami waves (arrival times minus the earthquake origin time) by backward ray tracing from each station (Fig. 5). The travel time curves ideally surround the tsunami source area. We used

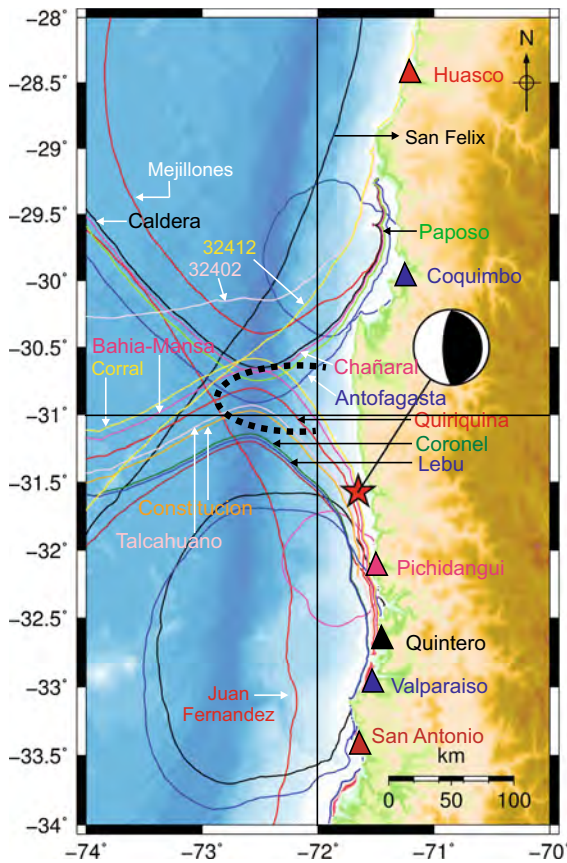


Figure 5

Backward ray tracing of the observed tsunamis. The *triangles* indicate the locations of tide gauges. The *line contours* show tsunami backward travel times from tide gauge or DART stations. The *same color* is used for the line contours, the names, and the triangles of the same stations, although some stations are located outside of the map. *Black dotted line* indicates the inferred tsunami source. Modified from Heidarzadeh et al. (2016)

30 arc s General Bathymetric Chart of the Oceans (GEBCO)-2014 bathymetric data, which has resolution of  $\sim 1$  km, and hence, finer topography or bathymetry features around the tide gauge stations cannot be expressed. Romano et al. (2016) estimated the optimal time shifts of tsunami waveforms recorded on coastal tide gauges as several minutes. Considering the uncertainties, we can roughly estimate the tsunami source at around  $31^\circ\text{S}$  and extending as far west as  $73^\circ\text{W}$ . Note that the eastern edge of the source is not constrained by the observed data; hence, the above estimate only limits the offshore side of the tsunami source. The main tsunami source seems to extend to the trench axis. Figure 5

does not support tsunami source south of the epicenter, i.e., offshore asperity III of Lee et al. (2016).

Lay et al. (2016) computed tsunamis from the slip models of Lee et al. (2016), including the offshore asperity III ruptured at 95 s, and found that the additional source cannot reproduce the observed tsunami waveforms at DART and coastal tide gauge stations. Heidarzadeh et al. (2016) also made tsunami simulation for such a long fault with a second asperity south of the epicenter, and concluded that the model predicted tsunami first arrivals at southern stations (Pichidangui, Quintero, Valparaiso and San Antonio, Constitucion) are not consistent with observations.

## 5. Conclusions

Like many other great earthquakes along the Chilean coast, the 2015 Illapel earthquake occurred in the same region as some previous events. The previous earthquakes in this region occurred in 1943 and 1880. The source regions of great earthquakes coincide with regions of high coupling as inferred from GPS measurements. The source models based on seismic, tsunami, and geodetic data are mostly similar: source duration of 100 s with a peak at 50 s and the largest slip at  $31^\circ\text{S}$ ,  $72^\circ\text{W}$ , approximately 70 km to the NW of the epicenter. The distribution of tsunami heights is consistent with the slip distribution. The large-slip area seems to be extended to the trench axis. Another deeper patch is proposed from high-frequency seismic waves. A model involving a secondary tsunami earthquake and a third asperity south of the epicenter is also proposed, but is not supported by tsunami data.

## Acknowledgements

We thank Alexander Rabinovich (Editor-in-Chief) for inviting us to contribute this review article. Tsunami data are downloaded from the sea-level station monitoring facility of Intergovernmental Oceanographic Commission (IOC) of UNESCO at: <http://www.ioc-sealevelmonitoring.org/>. Some figures are drafted using the GMT software of Wessel

and Smith (1998). DART data are provided by the National Oceanic and Atmospheric Administration (NOAA) of the United States (<http://www.ndbc.noaa.gov/dart.shtml>). This work was partially supported by KAKENHI (16H01838).

## REFERENCES

- Aránguiz, R., González, G., González, J., Catalan, P. A., Cienfuegos, R., Yagi, Y., et al. (2016). The 16 September 2015 Chile tsunami from the post-tsunami survey and numerical modeling perspectives. *Pure and Applied Geophysics*, *173*, 333–348.
- Atwater, B.F., Cisternas, M.V., Bourgeois, J., Dudley, W.C., Hendley II J.W., Stauffer, P.H. (1999). Surviving a tsunami—lessons from Chile, Hawaii, and Japan (p. 20). U.S. Geological Survey Circular 1187.
- Beck, S., Barrientos, S., Kausel, E., & Reyes, M. (1998). Source characteristics of historic earthquakes along the central Chile subduction zone. *Journal of South American Earth Sciences*, *11*, 115–129.
- Calisto, I., Miller, M., & Constanzo, I. (2016). Comparison between tsunami signals generated by different source models and the observed data of the Illapel 2015 earthquake. *Pure and Applied Geophysics*, *173*, 1051–1061.
- Comte, D., & Pardo, M. (1991). Reappraisal of great historical earthquakes in the northern Chile and southern Peru seismic gaps. *Natural Hazards*, *45*, 23–44.
- Contreras-López, M., Winckler, P., Sepúlveda, I., et al. (2016). Field Survey of the 2015 Chile tsunami with emphasis on coastal wetland and conservation areas. *Pure and Applied Geophysics*, *173*, 349–367.
- Fuentes, M., Riquelme, S., Hayes, G., Medina, M., Melgar, D., Vargas, G., et al. (2016). A study of the 2015 Mw 8.3 Illapel earthquake and tsunami: Numerical and analytical approaches. *Pure and Applied Geophysics*, *173*, 1847–1858.
- Fujii, Y., & Satake, K. (2013). Slip distribution and seismic moment of the 2010 and 1960 Chilean earthquakes inferred from tsunami waveforms and coastal geodetic data. *Pure and Applied Geophysics*, *170*, 1493–1509.
- Gusman, A. R., Murotani, S., Satake, K., Heidarzadeh, M., Gunawan, E., Watada, S., et al. (2015). Fault slip distribution of the 2014 Iquique, Chile, earthquake estimated from ocean-wide tsunami waveforms and GPS data. *Geophysical Research Letters*, *42*, 1053–1060.
- Hatori, T. (1968). Study on distant tsunamis along the coast of Japan, Part 2, tsunamis of South American origin. *Bulletin of the Earthquake Research Institute University Tokyo*, *46*, 345–359.
- Heidarzadeh, M., Murotani, S., Satake, K., Ishibe, S., & Gusman, A. R. (2016). Source model of the 16 September 2015 Illapel, Chile, Mw 8.4 earthquake based on teleseismic and tsunami data. *Geophysical Research Letters*, *43*, 643–650.
- Heidarzadeh, M., Satake, K., Murotani, S., Gusman, A. R., & Watada, S. (2015). Deep-water characteristics of the trans-Pacific tsunami from the 1 April 2014 Mw 8.2 Iquique, Chile earthquake. *Pure and Applied Geophysics*, *172*, 719–730.
- Kanamori, H. (1977). The energy release in great earthquakes. *Journal of Geophysical Research*, *82*, 2981–2987.
- Kelleher, J. A. (1972). Rupture zones of large South American earthquakes and some predictions. *Journal of Geophysical Research*, *77*, 2087–2103.
- Lay, T., Yue, H., Brodsky, E. E., & An, C. (2014). The 1 April 2014 Iquique, Chile, Mw 8.1 earthquake rupture sequence. *Geophysical Research Letters*, *41*, 3818–3825.
- Lee, S.-J., Yeh, T.-Y., Lin, T.-C., Lin, Y.-Y., Song, T.-R. A., & Huang, B.-S. (2016). Two-stage composite megathrust rupture of the 2015 Mw8.4 Illapel, Chile, earthquake identified by spectral-element inversion of teleseismic waves. *Geophysical Research Letters*, *43*, 4979–4985.
- Li, B., & Ghosh, A. (2016). Imaging rupture process of the 2015 Mw 8.3 Illapel earthquake using the US Seismic Array. *Pure and Applied Geophysics*, *173*, 2245–2255.
- Li, L., Lay, T., Cheung, K. F., & Ye, L. (2016). Joint modeling of teleseismic and tsunami wave observations to constrain the 16 September 2015 Illapel, Chile, Mw 8.3 earthquake rupture process. *Geophysical Research Letters*, *43*, 4303–4312.
- Madariaga, R., Metois, M., Vigny, C., & Campos, J. (2010). Central Chile Finally Breaks. *Science*, *328*, 181–182.
- Melgar, D., Fan, W., Riquelme, S., Geng, J., Liang, C., Fuentes, M., et al. (2016). Slip segmentation and slow rupture to the trench during the 2015, Mw8.3 Illapel, Chile earthquake. *Geophysical Research Letters*, *43*, 961–966.
- Métouis, M., Vigny, C., & Socquet, A. (2016). Interseismic coupling, megathrust earthquakes and seismic swarms along the Chilean subduction zone (38°–18°S). *Pure and Applied Geophysics*, *173*, 1431–1449.
- Moreno, M., Rosenau, M., & Onken, O. (2010). 2010 Maule earthquake slip correlates with pre-seismic locking of Andean subduction zone. *Nature*, *467*, 198–202.
- Okuwaki, R., Yagi, Y., Aránguiz, R., González, J., & González, G. (2016). Rupture process during the 2015 Illapel, Chile earthquake: Zigzag-along-dip rupture episodes. *Pure and Applied Geophysics*, *173*, 1011–1020.
- Omira, R., Baptista, M. A., & Lisboa, F. (2016). Tsunami characteristics along the Peru-Chile trench: Analysis of the 2015 Mw8.3 Illapel, the 2014 Mw8.2 Iquique and the 2010 Mw8.8 Maule tsunamis in the near-field. *Pure and Applied Geophysics*, *173*, 1063–1077.
- Romano, F., Piatanesi, A., Lorito, S., Tolomei, C., Atzori, S., & Murphy, S. (2016). Optimal time alignment of tide-gauge tsunami waveforms in nonlinear inversions: Application to the 2015 Illapel (Chile) earthquake. *Geophysical Research Letters*, *43*, 11226–11235. doi:10.1002/2016GL071310.
- Ruiz, S., Klein, E., del Campo, F., Rivera, E., Poli, P., Métouis, M., et al. (2016). The seismic sequence of the 16 September 2015 Mw 8.3 Illapel, Chile, earthquake. *Seismological Research Letters*, *87*, 789–799.
- Schurr, B., Asch, G., Hainzl, S., Bedford, J., Hoechner, A., Palo, M., et al. (2014). Gradual unlocking of plate boundary controlled initiation of the 2014 Iquique earthquake. *Nature*, *512*, 299–302.
- Tang, L., Titov, V. V., Moore, C., & Wei, Y. (2016). Real-time assessment of the 16 September 2015 Chile tsunami and implications for near-field forecast. *Pure and Applied Geophysics*, *173*, 369–387.
- Tilmann, F., Zhang, Y., Moreno, M., Saul, J., Eckelmann, F., Palo, M., et al. (2016). The 2015 Illapel earthquake, central Chile: A type case for a characteristic earthquake? *Geophysical Research Letters*, *43*, 574–583.



A Review of Source Models of the 2015 Illapel, Chile Earthquake and Insights

- Watanabe, H. (1998). *Materials for comprehensive list of destructive tsunamis in Japan* (“*Nihon Higai Tsunami Souran*”) (p. 206). Tokyo: University of Tokyo Press.
- Wessel, P., & Smith, W. H. F. (1998). New, improved version of Generic Mapping Tools released. *EOS Transactions, AGU*, 79, 579.
- Ye, L., Lay, T., Kanamori, H., & Koper, K. D. (2016). Rapidly estimated seismic source parameters for the 16 September 2015 Illapel, Chile Mw 8.3 earthquake. *Pure and Applied Geophysics*, 173, 321–332.
- Yoshimoto, M., Watada, S., Fujii, Y., & Satake, K. (2016). Source estimate and tsunami forecast from far-field deep-ocean tsunami waveforms—The 27 February 2010 Mw 8.8 Maule earthquake. *Geophysical Research Letters*, 43, 659–665.
- Zaytsev, O., Rabinovich, A. B., & Thomson, R. E. (2016). A comparative analysis of coastal and open-ocean records of the great Chilean tsunamis of 2010, 2014 and 2015 off the coast of Mexico. *Pure and Applied Geophysics*. doi:10.1007/s00024-016-1407-8.
- Zhang, Y., Zhang, G., Hetland, E. A., Shan, X., Wen, S., & Zuo, R. (2016). Coseismic fault slip of the September 16, 2015 Mw 8.3 Illapel, Chile earthquake estimated from InSAR data. *Pure and Applied Geophysics*, 173, 1029–1038.

(Received November 3, 2016, revised November 30, 2016, accepted December 1, 2016)